Identification and Crystallographic Analysis of a New Carbohydrate Acetylesterase (SmAcE1) from *Sinorhizobium meliloti*

Changsuk Oh [1], Bum Han Ryu [1], Wanki Yoo [1], Duy Duc Nguyen [1], Truc Kim [1] , Sung-Chul Ha [2], T. Doohun Kim [3,*] and Kyeong Kyu Kim [1,*]

[1] Department of Molecular Cell Biology, Samsung Medical Center, Sungkyunkwan University School of Medicine, Suwon 16419, Korea; changs.oh@gmail.com (C.O.); psryubh@gmail.com (B.H.R.); vlqkshqk61@outlook.kr (W.Y.); clara-y@hanmail.net (D.D.N.); kdttruc83@gmail.com (T.K.)

[2] Beamline Department, Pohang Accelerator Laboratory, Pohang University of Science and Technology, Pohang 37673, Korea; scha2@postech.ac.kr

[3] Department of Chemistry, College of Natural Sciences, Sookmyung Woman's University, Seoul 04310, Korea

* Correspondence: doohunkim@sookmyung.ac.kr (T.D.K.); kyeongkyu@skku.edu (K.K.K.)

Abstract: Carbohydrate-active enzymes (CAZymes) regulate the synthesis, degradation, and modification of the poly—and oligosaccharides in all three kingdoms of life. A novel carbohydrate acetylesterase from *Sinorhizobium meliloti*, designated SmAcE1, was identified, characterized, and crystallized. This SmAcE1 is classified into the carbohydrate esterase family 3 (CE3) based on the sequence alignments with other currently known carbohydrate esterase (CE) family enzymes. The SmAcE1 was crystallized as a hexamer in a space group $P2_12_12_1$ with the unit cell parameters: a = 99.12 Å, b = 148.88 Å, c = 149.84 Å, and $\alpha = \beta = \gamma = 90.00°$. The diffraction data set was collected up to a 2.05 Å resolution. Hydrolysis activity of SmAcE1 towards glucose pentaacetate and cellulose acetate was further confirmed using acetic acid release assay. Further crystallographic and functional analyses studies on SmAcE1 would be followed to fully understand the reaction mechanisms of CEs.

1. Introduction

Carbohydrate active enzymes (CAZymes) synthesize, degrade, and modify poly—or oligo saccharide chain, including cell wall not only in plant, but also in bacteria and fungi [1–4]. Among these proteins, carbohydrate esterases (CEs) play key roles in making other CAZymes access their carbohydrate substrates by removing acetyl groups from substituted saccharides with various chain lengths [5,6]. In the physiological aspect, CEs are considered to be involved in the formation of cell walls, interactions between host and microbes, and energy metabolism pathways [7–15]. CEs are also important for biotechnological application, as modifications of carbohydrates are necessary for the preparation of biofuel, drug carriers, and cosmetics [16–18]. To date, based on the sequence similarities and the presence of characteristic carbohydrate binding modules, CEs can be classified into fifteen subfamilies from CE1 to CE16.

Bacterial CEs have important physiological functions, which were proven by that the CE mutant shows growth retardation [19,20]. However, only few bacterial CEs have been identified and investigated in detail. For example, CEs from *Geobacillus stearothermophilus*, *Butyrivibrio proteoclasticus*, *Neisseria gonorrhoeae*, and *Escherichia coli* 0157 were characterized in the biochemical and structural aspects [21–24]. Most CEs belong to α/β-hydrolase family and show broad substrate specificity, but detailed reaction and substrate recognition mechanisms in the atomic levels have not been

well studied yet. Therefore, it is necessary to execute structural and biochemical investigations of bacterial CEs in order to understand their reaction mechanism as well as substrate specificity, which will eventually contribute to full understanding of their physiological roles as well as their biotechnological applications.

In this study, based on the sequence identity with other known CE3 family enzymes, we identified a novel carbohydrate acetylesterase (SmAcE1) in CE3 family from *Sinorhizobium meliloti*, a nitrogen-fixing soil bacterium. We further characterized and crystallized the recombinant SmAcE1, which will pave a way for understanding of the catalytic mechanism as well as structural features of CE family members.

2. Materials and Methods

2.1. Materials

All of the reagents were purchased from Sigma-Aldrich (St. Louis, MO, USA) unless specified otherwise, and all of the chromatography columns were purchased from GE Healthcare (Chicago, IL, USA).

2.2. Sequence Alignment of SmAcE1 with Other CEs

Sequence alignment was performed using CE3 family members whose structures are currently known. Sm23 (PDB code: 4TX1, [25]), Est24 (PDB code: 5HOE [26]), TcAE206 (PDB code: 5B5S [27]), and CtCES3-1 (PDB code: 2TVP [28]) were used. Furthermore, CtCE2 from *Clostridium thermocellum* (PDB code: 2WAO [29]) that belongs to the CE2 was also included for the sequence alignment [30,31]. Amino acid sequences were obtained from UniProt (http://www.uniprot.org/) and sequence alignment was done using PROMALS3D [32] and were visualized using ESPript [33].

2.3. Cloning and Site-Directed Mutagenesis

A gene SMa2002, encoding for SmAcE1 (NCBI: NP_436343.1), was amplified from the pSymA megaplasmid of the soil bacteria S. meliloti 1021 (Korean Collection for Type Cultures, KCTC) by polymerase chain reaction (PCR) using the primer pair: 5′-GC GGA TCC ATG GAG GAG ACA GTG-3′ and 5′-GC AAG CTT TTA CGC ATC GGG CCA-3′ (BamHI and HindIII sites are underlined). The PCR product was then digested by BamHI and HindIII (NEB, Ipswich, MA, USA) and were inserted into the corresponding sites of the expression vector pQE30 (Qiagen, Hilden, Germany). The deduced recombinant SmAcE1 sequence contains 12 amino acids of the hexa-His tag (MRGSHHHHHHGS) in *N*-terminus and 220 amino acids of the full-length SmAcE1 was followed.

To generate an inactive mutant of SmAcE1, Ser[15] was replaced by Ala using Quick-Change site-directed mutagenesis kit (Stratagene, La Jolla, CA, USA) and the primer pair: 5′-CGT TCT ATG CTT CGG AGA TGC CAA CAC TCA CGG CC-3′ and 5′-GGC CGT GAG TGT TGG CAT CTC CGA AGC ATA GAA CG-3′.

2.4. Protein Expression and Crystallization

Escherichia coli XL1-Blue (Stratagene, La Jolla, CA, USA) harboring pQE30-SmAcE1 was cultured at 310 K until the OD_{600} reached 0.5–0.7. To induce the expression of SmAcE1, isopropyl β-D-1-thiogalactopyranoside (IPTG) was added into bacterial culture at a final concentration of 1 mM. After culturing for an additional 4 h at 310 K, cells were harvested, resuspended in buffer A (50 mM Tris pH 8.0, 300 mM NaCl and 50 mM imidazole), and lysed by sonication (300 short bursts of 1 s followed by intervals of 3 s) on ice. After centrifugation at $16,000 \times g$ for 1 h, the supernatant was loaded onto a 5-mL Ni-NTA column. The column was washed with 50 mL of buffer A to remove the non-specifically bound proteins, and the bound proteins were eluted using a linear gradient of 50–500 mM imidazole in buffer A. Fractions containing SmAcE1 were collected, and were then loaded onto a HiLoad 16/600 Superdex 200 column pre-equilibrated with 10 mM Tris-HCl pH 8.0.

The purified SmAcE1 was concentrated to 5 mg·mL^{-1} and stored at 193 K for further use. The SmAcE1 S15A mutant was purified using the same procedure as the wild type.

The purified SmAcE1 was crystallized using the microbatch method, by mixing 1 μL of protein (5 mg·mL^{-1}) with 1 μL of mother liquor on a Nunc 72-well plate (Thermo Fisher Scientific, Roskilde, Denmark) under the Al's Oil (Hampton Research, Aliso Viejo, CA, USA). Initial crystallization screening was performed using Crystal Screen I, Crystal Screen II, Crystal Screen Cryo, and StockOptions Salt Kits at 295 K. The crystallization conditions were further optimized by changing salt concentration and adding additives using the Additive Screen Kit (Hampton Research, Aliso Viejo, CA, USA).

2.5. Data Collection

Prior to data collection, a single SmAcE1 crystal was soaked into the mother liquor containing 50% glycerol and were flash cooled under a cryostream of nitrogen gas at 100 K. Diffraction data of SmAcE1 crystal were collected over a total range of 360° using 1° oscillations and an exposure time of 2 s on an ADSC Q315r detector at the beamline 5C of Pohang Acceleration Laboratory (Korea). The collected data were processed using HKL2000 [34]. The data collection statistics are described in Table 1.

Table 1. Data collection and processing statistics.

Data Collection	
Space group	$P2_12_12_1$
Wavelength (Å)	1.0000
Resolution range (Å)	47.35–2.05 (2.12–2.05)
Unit cell	
a, b, c (Å)	99.12, 148.88, 149.84
α, β, γ (°)	90.00, 90.00, 90.00
R_{merge} (%)	12.8 (51.05)
No. of unique reflections	137748 (13410)
Completeness (%)	98.91 (97.41)
Mean I/σ	11.47 (3.28)
[1] $CC_{1/2}$	0.996 (0.925)
[2] CC*	0.999 (0.980)
Redundancy	8.9 (7.8)
Wilson B-factor	16.16

Score in the bracket were in the highest resolution shell. [1] $CC_{1/2}$ is the correlation coefficient between two random half data sets. [2] CC* = $\sqrt{\{2CC_{1/2}/(1 + CC_{1/2})\}}$.

2.6. Analytical Size-Exclusion Chromatography

To analyze the oligomeric state of SmAcE1, purified SmAcE1 (0.5 mg·mL^{-1}) was loaded onto a Superdex 200 10/300 GL column equilibrated with buffer containing 10 mM Tris-HCl, pH 8.0, and 100 mM NaCl. Purified Est-Y29 (354 kDa) [35] and other molecular-weight marker proteins (ferritin, 440 kDa; aldolase, 158 kDa) from Gel Filtration Calibration Kits (GE Healthcare, Chicago, IL, USA) were used to calculate the molecular weight of SmAcE1, following the manufacturer's instructions. Injected volumes of all the samples were 200 μL.

2.7. Enzyme Activity Assay Using Colorimetric Method

Carbohydrate deacetylase activity of SmAcE1 was analyzed by observing the color change of Phenol Red, a pH indicator, upon the release of acetate from carbohydrate substrates. Stock solution of glucose pentaacetate (5 mg·mL^{-1}) was prepared in dimethyl sulfoxide, whereas stock solution of cellulose acetate (1 mg·mL^{-1}) was prepared in acetone. These two chemicals (50 ng each) were incubated with 100 ng SmAcE1 wild type or S15A mutant in a reaction buffer containing 10 mM Tris pH 8.0 and 20% Phenol Red in a 96-well plate at 297 K. The plate was photographed after 15 min.

3. Results and Discussion

The sequence of SmAcE1 was compared with other CE3s, whose structures were currently known (Figure 1). In addition, the sequence of CtCE2, was also included in the sequence alignment. Since CtCE2 is the only CE whose complex structure with carbohydrate was identified, we expected the sequence comparison between SmAcE1 and CtCE2 can provide useful information to understand the carbohydrate-SmAcE1 interaction. Sequence alignment of SmAcE1 with other CEs revealed that GDS(L) motif is conserved not only in CE3s (Sm23, EST24, CtCES3-1, and TcAE206), but also in CE2 (CtCE2). Among catalytic triads (Ser-His-Asp), catalytic serine as a nucleophile is conserved in GDSL motif, and other residues, His and Asp, are positioned in DXXH motif as same with other CEs. Based on the sequence alignment of SmAcE1 with other known CEs (Figure 1), Ser[15], positioned in GDSL motif of SmAcE1 is considered as the active nucleophile. Accordingly, we mutated this residue to Ala ad check the hydrolysis activity of the mutant for confirming this hypothesis. Oxyanion hole components (Ser, Gly/Ala, Asn, and His) in the known CE3 (Est24, Sm23, CtCES3_1, and TcAE206) are also conserved in CtCE2 and SmAcE1 (Figure 1) [27–31]. From these analyses, it can be proposed that SmAcE1 possibly has a similar catalytic mechanism to the known carbohydrate esterases belonging to CE2 and CE3. A few residues in SmAcE1, such as Asp[64], showed difference with carbohydrate-binding residues in CtCE2 [27] (Figure 1). It suggests that residue for carbohydrate-recognition of SmAcE1 might be little different from that of CtCE2.
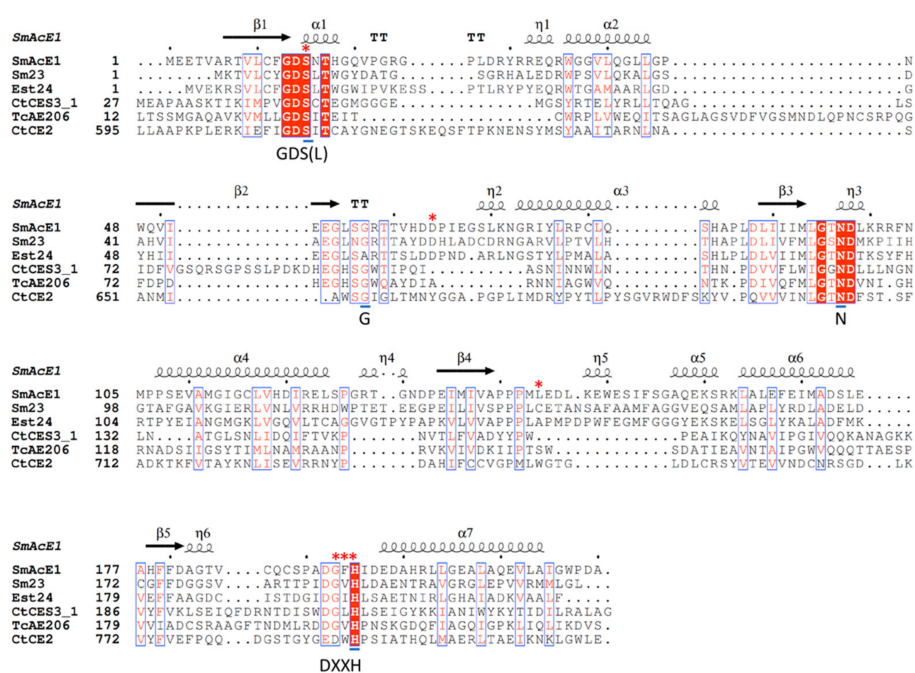

Figure 1. Sequence alignment of carbohydrate esterases. Sequence of SmAcE1 was compared with other structurally identified CEs (CE2: CtCE2 and CE3: Sm23, Est24, CtCES3-1 and TcAE206). In sequence alignment, only esterase domains were used for CtCE2 [29], CtCES3-1, and TcAE206, and the full sequence was used for SmAcE1. The predicted secondary structure of SmAcE1 was displayed on top of the aligned, and GDS(L) and DXXH motifs, which contain catalytic triad (Ser[15], Asp[195] and His[192]), were marked with motif names under each position. The oxyanion hole residues were highlighted using the blue bar and their name under the residues. The β-D-glucose-binding residues (Ser[612], Tyr[665], Trp[746], Asp[789], Trp[790], and His[791]) in CtCE2 complex (PDB code: 2WOA [29]) were marked using red asterisks. Sequence identities of Sm23, Est24, CtCE2, CtCES3-1, and TcAE206 to SmAcE1 were 30.3%, 32.5%, 10.6%, 12.4%, and 9.5%, and sequence similarities of Sm23, Est24, CtCE2, CtCES3-1, and TcAE206 to SmAcE1 were 41.2%, 44.2%, 26.3%, 26.3%, and 22.6% in 274 of length of multiple sequence alignment.

To structurally and functionally characterize SmAcE1, recombinant SmAcE1 was heterologously expressed in *E. coli* and purified with a high purity (Figure 2A). Molecular weight, judged by SDS-PAGE analysis, is similar to theoretical molecular weight (25.7 kDa) of the recombinant SmAcE1 (Figure 2A). The oligomeric state of SmAcE1 was estimated using analytical size-exclusion chromatography. The elution volume of SmAcE1 was compared with those of the molecular-weight markers, ferritin from horse spleen (440 kDa), Est-Y29 from metagenomics library (354 kDa), and aldolase from rabbit muscle (158 kDa) (Figure 2B). Based on size-exclusion chromatography, molecular weight of SmAcE1 was calculated to be ~185 kDa. When considering the molecular weight of the monomeric SmAcE1 (25.7 kDa), SmAcE1 forms a heptamer in solution. However, when considering the experimental error in the size-exclusion chromatography and oligomeric state of other known CEs, we cannot exclude the possibility of forming a hexamer or an octamer. To get a better insight into the oligomeric state and the structure of SmAcE1, we crystallized SmAcE1 and examined its packing in the crystal.
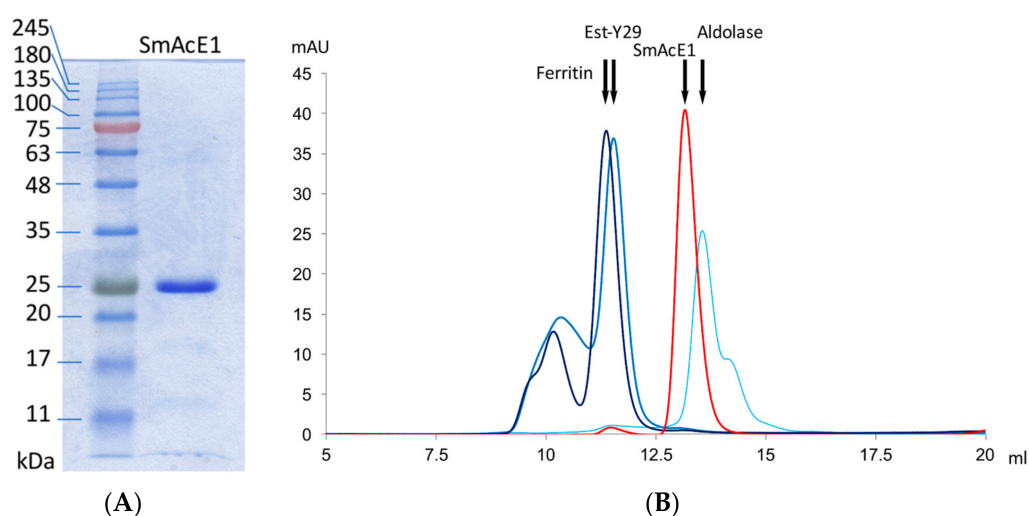

Figure 2. Characterization of the recombinant SmAcE1. (**A**) SDS-PAGE analysis of the purified SmAcE1. Molecular weight of purified SmAcE1 was estimated on SDS-PAGE analysis. The mobility of the protein size markers and SmAcE1 were displayed in first and the second lanes, respectively. The protein band of SmAcE1 is closely located to 25.7 kDa. (**B**) Analytical size-exclusion chromatography of SmAcE1 (red). Retention peaks of ferritin (440 kDa, deep blue), Est-Y29 (354 kDa, blue), and aldolase (158 kDa, light blue) were marked using black arrows. Molecular weight of SmAcE1 was estimated as ~185 kDa. Void volume of the column is 8.2 mL.

In the initial crystallization screen, crystals of SmAcE1 were obtained in the presence of 2.5 M ammonium citrate. To obtain diffraction-quality crystals, further screening was tried with Additive Screen kit and Salt Screen Kit. Finally, the diffraction-quality crystals were obtained from 2.0 M ammonium citrate with 1% ethyl acetate. The orthorhombic crystals grew to the final dimensions of about $1.2 \times 0.4 \times 0.4$ mm within three weeks (Figure 3A). Crystals were diffracted to ~2.0 Å resolution (Figure 3B). The diffraction data set was collected and processed with 98.9% completeness to 2.05 Å resolution (Table 1). R_{merge} of the data set is 12.8% and overall redundancy is 8.9. The SmAcE1 crystal belongs to an orthorhombic space group $P2_12_12_1$ with the unit cell parameters a = 99.12 Å, b = 148.88 Å, c = 149.84 Å, $\alpha = \beta = \gamma = 90.00°$, and a calculated unit cell volume of 2.21×10^6 Å^3. The presence of hexameric SmAcE1 in an asymmetric unit gives a calculated Matthews coefficient V_M of 3.58 Å^3 Da^{-1}, which corresponds to a solvent content of 65.65%. The V_M is within a range frequently observed in protein crystals [36–38].
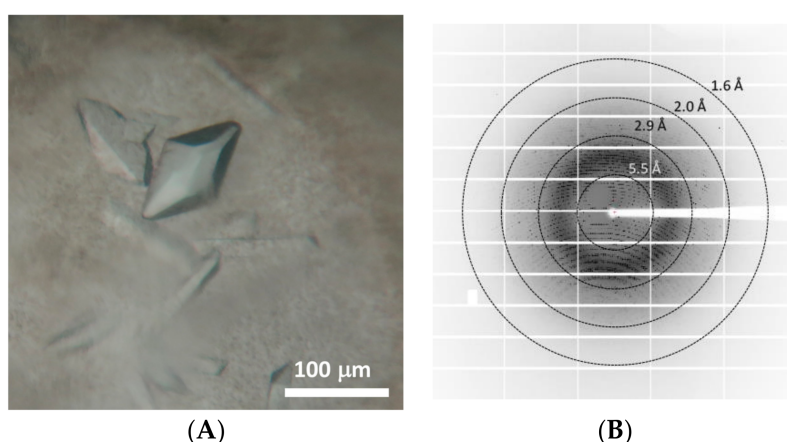
Figure 3. Crystals of SmAcE1 and the representative diffraction pattern. (**A**) SmAcE1 crystal image with a white scale bar indicating 100 μm length. The black-arrow directing crystal was used for data collection. (**B**) Representative diffraction image of SmAcE1 crystal. Resolutions (1.6 Å, 2.0 Å, 2.9 Å, 5.5 Å) are marked using dotted line as concentric circles on proper position. Beam center is marked using a red cross. Diffraction image was prepared using the Adxv software [39].

For structural studies, we used molecular replacement (MR) method and the program Phaser [40] to search for the structure solution. Because Est24 from *S. meliloti* showed the high sequence identity (43% in 215 of alignment length) to SmAcE1 (Figure 1), Est24 crystal structure (PDB code: 5HOE [26]) was used as a search template. From the result of Phaser, we obtained a solution with a top log-likelihood gain (LLG), and a top translation function Z-score (TFZ) value of 5940 and 57.4, respectively, indicating that we identified an unambiguous structure solution. Subsequent refinement combined with model building using *phenix.refine* [41] and *Coot* [42], respectively, revealed a model with R_{factor} and R_{free} values of 13.6% and 16.0%, respectively, at 2.05 Å resolution. From this model, we identified that six molecules of SmAcE1 exist as a hexameric oligomer in an asymmetric unit (Figure 4), suggesting that SmAcE1 forms a hexamer, instead of a heptamer, in the solution. The solution from MR will facilitate our further progress to complete the crystal structure of SmAcE1.
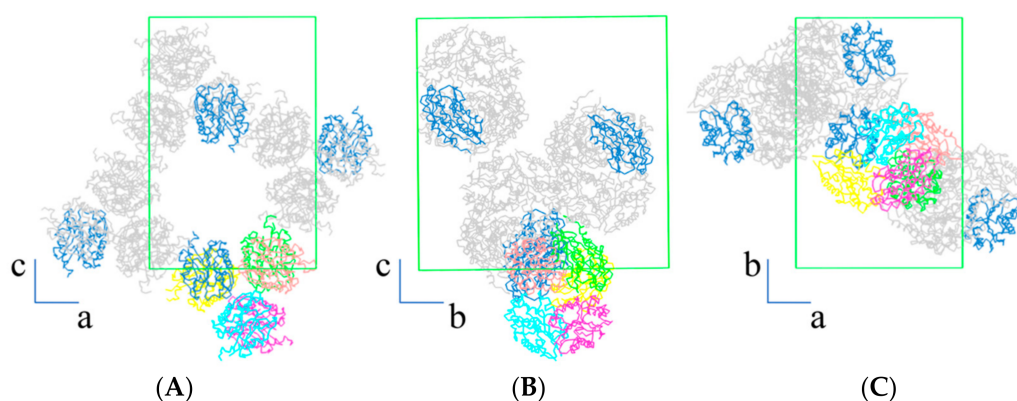

Figure 4. Crystal packing of SmAcE1. SmAcE1 in crystal lattice of the orthorhombic $P2_12_12_1$ crystals on a-c plane (**A**), b-c plane (**B**), and a-b plane (**C**) were shown as ribbons. Molecules in an asymmetric unit form a hexamer and are colored green, cyan, magenta, salmon, yellow, and blue; whereas, symmetry-related molecules are colored grey. To clearly define the symmetry-related hexamers, the corresponding SmAcE1 molecules in each hexamer are colored blue as the reference points. The unit cell boundaries are defined using green lines.

To examine the carbohydrate acetylesterase activity of the recombinant SmAcE1, two acetylated carbohydrates were employed as substrates: glucose pentaacetate and cellulose acetate. The catalytic activity of SmAcE1 was confirmed by the phenol red color assay, in which the color of solution turns yellow as the pH is lowered by the hydrolyzed acetates from the substrates. As shown in Figure 5, the wild-type SmAcE1 showed acetylesterase activity towards both substrates by showing the color change to yellow (Figure 5B,E) when compared to the control (Figure 5A,D). However, the mutant SmAcE1 (SmAcE1 S15A) did not show any color changes (Figure 5C,F).
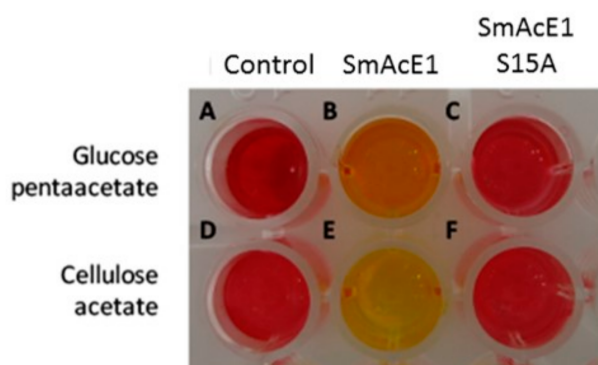

Figure 5. Carbohydrate acetylesterase activity to acetylated carbohydrates. The hydrolysis activity of SmAcE1 on two acetylated carbohydrate substrates, glucose pentaacetate (**A**–**C**) and cellulose acetate (**D**–**F**) was tested in the absence of enzyme (**A**,**D**), and the presence of the wild-type SmAcE1 (**B**,**E**) and the inactive mutant S15A of SmAcE1 (**C**,**F**). After hydrolysis, the produced acetate in solution changes the color from red to yellow.

From the functional and structural analyses of Sm23 and Est24, their substrate specificity has not been well understood in atomic levels due to the lack of the substrate-bound structures [25,26,29]. On the other hand, the crystal structure of CtCE2 in a complex with β-D-glucose chain (PDB code: 2WAO) showed how CEs recognize their carbohydrate substrates. Based on the sequence alignment, the crucial motifs that are required for catalytic activity and components of oxyanion hole are well conserved in the carbohydrate esterases of CE2 and CE3. Accordingly, the structural comparison of SmAcE1 to the carbohydrate-bound CtCE2 will provide crucial information on how SmAcE1 recognizes carbohydrate substrates, and will show the molecular basis of broad substrate specificity in SmAcE1. Collectively, current study will pave a way in obtaining structural and functional insights into carbohydrate acetylesterases of CE3.

Author Contributions: Bum Han Ryu, Wanki Yoo, and T. Doohun Kim identified genes from the chromosome of *Sinorhizobium meliloti*. Bum Han Ryu and Wanki Yoo cloned the gene in the expression vector and made a mutant. Changsuk Oh, Duy Duc Nguyen, and Truc Kim purified, characterized and crystallized proteins. Changsuk Oh, Truc Kim and Sung-Chul Ha collected and analyzed the diffraction data. T. Doohun Kim and Kyeong Kyu Kim coordinated the project. Changsuk, T. Doohun Kim and Kyeong Kyu Kim wrote the manuscript. All authors reviewed the results and approved the final version of the manuscript.

Conflicts of Interest: The authors declare no conflict of interest.

References

1. Andre, I.; Potocki-Véronèse, G.; Barbe, S.; Moulis, C.; Remaud-Siméon, M. CAZyme discovery and design for sweet dreams. *Curr. Opin. Chem. Biol.* **2014**, *19*, 17–24. [CrossRef] [PubMed]

2. Cantarel, B.L.; Coutinho, P.M.; Rancurel, C.; Bernard, T.; Lombard, V.; Henrissat, B. The Carbohydrate-Active EnZymes database (CAZy): An expert resource for Glycogenomics. *Nucleic Acids Res.* **2009**, *37*, D233–D238. [CrossRef] [PubMed]

3. Coutinho, P.M.; Stam, M.; Blanc, E.; Henrissat, B. Why are there so many carbohydrate-active enzyme-related genes in plants? *Trends Plant Sci.* **2003**, *8*, 563–565. [CrossRef] [PubMed]

4. Ekstrom, A.; Taujale, R.; McGinn, N.; Yin, Y. PlantCAZyme: A database for plant carbohydrate-active enzymes. *Database* **2014**. [CrossRef] [PubMed]

5. Adesioye, F.A.; Makhalanyane, T.P.; Biely, P.; Cowan, D.A. Phylogeny, classification and metagenomic bioprospecting of microbial acetyl xylan esterases. *Enzyme Microb. Technol.* **2016**, *93–94*, 79–91. [CrossRef] [PubMed]

6. Wong, D.W. Feruloyl esterase: A key enzyme in biomass degradation. *Appl. Biochem. Biotechnol.* **2006**, *133*, 87–112. [CrossRef]

7. Barad, S.; Sela, N.; Kumar, D.; Kumar-Dubey, A.; Glam-Matana, N.; Sherman, A.; Prusky, D. Fungal and host transcriptome analysis of pH-regulated genes during colonization of apple fruits by *Penicillium expansum*. *BMC Genom.* **2016**, *17*, 330. [CrossRef] [PubMed]

8. Busse-Wicher, M.; Gomes, T.C.F.; Tryfona, T.; Nikolovski, N.; Stott, K.; Grantham, N.J.; Bolam, D.N.; Skaf, M.S.; Dupree, P. The pattern of xylan acetylation suggests xylan may interact with cellulose microfibrils as a twofold helical screw in the secondary plant cell wall of *Arabidopsis thaliana*. *Plant J.* **2014**, *79*, 492–506. [CrossRef] [PubMed]

9. Chebli, Y.; Geitmann, A. Cellular growth in plants requires regulation of cell wall biochemistry. *Curr. Opin. Cell Biol.* **2017**, *44*, 28–35. [CrossRef] [PubMed]

10. Coque, L.; Neogi, P.; Pislariu, C.; Wilson, K.A.; Catalano, C.; Avadhani, M.; Sherrier, D.J.; Dickstein, R. Transcription of ENOD8 in medicago truncatula nodules directs ENOD8 esterase to developing and mature symbiosomes. *Mol. Plant-Microbe Interact.* **2008**, *21*, 404–410. [CrossRef] [PubMed]

11. Dickstein, R. ENOD8, a novel early nodule-specific gene, is expressed in empty alfalfa nodules. *Mol. Plant-Microbe Interact.* **1993**, *6*, 715–721. [CrossRef] [PubMed]

12. Grantham, N.J.; Wurman-Rodrich, J.; Terrett, O.M.; Lyczakowski, J.; Stott, K.; Iuga, D.; Simmons, T.J.; Durand-Tardif, M.; Brown, S.P.; Dupree, R.; et al. An even pattern of xylan substitution is critical for interaction with cellulose in plant cell walls. *Nat. Plants* **2017**. [CrossRef] [PubMed]

13. Jones, K.M.; Kobayashi, H.; Davies, B.W.; Taga, M.E.; Walker, G.C. How rhizobial symbionts invade plants: The Sinorhizobium–Medicago model. *Nat. Rev. Microbiol.* **2007**, *5*, 619–633. [CrossRef] [PubMed]

14. Kabel, M.A.; Yeoman, C.J.; Han, Y.; Dodd, D.; Abbas, C.A.; de Bont, J.M.; Morrison, M.; Cann, I.K.O.; Mackie, R.I. Biochemical characterization and relative expression levels of multiple carbohydrate esterases of the xylanolytic rumen bacterium Prevotella ruminicola 23 grown on an ester-enriched substrate. *Appl. Environ. Microbiol.* **2011**, *77*, 5671–5681. [CrossRef] [PubMed]

15. Zhang, B.; Zhang, L.; Li, F.; Zhang, D.; Liu, X.; Wang, H.; Xu, Z.; Chu, C.; Zhou, Y. Control of secondary cell wall patterning involves xylan deacetylation by a GDSL esterase. *Nat. Plants* **2017**, *3*, 17017. [CrossRef] [PubMed]

16. Antonopoulou, I.; Varriale, S.; Topakas, E.; Rova, U.; Christakopoulos, P.; Faraco, V. Enzymatic synthesis of bioactive compounds with high potential for cosmeceutical application. *Appl. Microbiol. Biotechnol.* **2016**, *100*, 6519–6543. [CrossRef] [PubMed]

17. Mathew, M.P.; Tan, E.; Shah, S.; Bhattacharya, R.; Adam Meledeo, M.; Huang, J.; Espinoza, F.A.; Yarema, K.J. Extracellular and intracellular esterase processing of SCFA–hexosamine analogs: Implications for metabolic glycoengineering and drug delivery. *Bioorg. Med. Chem. Lett.* **2012**, *22*, 6929–6933. [CrossRef] [PubMed]

18. Yeoman, C.J.; Han, Y.; Dodd, D.; Schroeder, C.M.; Mackie, R.I.; Cann, I.K. Thermostable enzymes as biocatalysts in the biofuel industry. *Adv. Appl. Microbiol.* **2010**, *70*, 1–55. [PubMed]

19. Kahya, F.H.; Andrew, P.W.; Yesilkaya, H. Deacetylation of sialic acid by esterases potentiates pneumococcal neuraminidase activity for mucin utilization, colonization and virulence. *PLoS Pathog.* **2017**, *13*, e1006263. [CrossRef] [PubMed]

20. Steenbergen, M.S.; Jirik, J.L.; Vimr, E.R. YjhS (NanS) is required for *Escherichia coli* to grow on 9-*O*-acetylated *N*-acetylneuraminic acid. *J. Bacteriol.* **2009**, *191*, 7134–7139. [CrossRef] [PubMed]

21. Pfeffer, J.M.; Weadge, J.T.; Clarke, A.J. Mechanism of action of *Neisseria gonorrhoeae O*-acetylpeptidoglycan esterase, an SGNH serine esterase. *J. Biol. Chem.* **2013**, *288*, 2605–2613. [CrossRef] [PubMed]

22. Rangarajan, E.S.; Ruane, K.M.; Proteau, A.; Schrag, J.D.; Valladares, R.; Gonzalez, C.F.; Gilbert, M.; Yakunin, A.F.; Cygler, M. Structural and enzymatic characterization of NanS (YjhS), a 9-*O*-Acetyl *N*-acetylneuraminic acid esterase from *Escherichia coli* O157:H7. *Protein Sci.* **2011**, *20*, 1208–1219. [CrossRef] [PubMed]

23. Till, M.; Goldstone, D.C.; Attwood, G.T.; Moon, C.D.; Kelly, W.J.; Arcus, V.L. Structure and function of an acetyl xylan esterase (Est2A) from the rumen bacterium *Butyrivibrio* proteoclasticus. *Proteins Struct. Funct. BioInform.* **2013**, *81*, 911–917. [CrossRef] [PubMed]

24. Lansky, S.; Alalouf, O.; Solomon, H.V.; Alhassid, A.; Govada, L.; Chayen, N.E.; Belrhali, H.; Shoham, Y.; Shoham, G. A unique octameric structure of Axe2, an intracellular acetyl-xylooligosaccharide esterase from *Geobacillus stearothermophilus*. *Acta Crystallogr. Sect. D Biol. Crystallogr.* **2014**, *70*, 261–278. [CrossRef] [PubMed]

25. Kim, K.; Ryu, B.H.; Kim, S.S.; An, D.R.; Ngo, T.D.; Pandian, R.; Kim, K.K.; Kim, T.D. Structural and biochemical characterization of a carbohydrate acetylesterase from *Sinorhizobium meliloti* 1021. *FEBS Lett.* **2014**, *589*, 117–122. [CrossRef] [PubMed]

26. Oh, C.; Ryu, B.H.; An, D.R.; Nguyen, D.D.; Yoo, W.; Kim, T.; Ngo, T.D.; Kim, H.S.; Kim, K.K.; Kim, T.D. Structural and biochemical characterization of an octameric carbohydrate acetylesterase from *Sinorhizobium meliloti*. *FEBS Lett.* **2016**, *590*, 1242–1252. [CrossRef] [PubMed]

27. Watanabe, M.; Fukada, H.; Inoue, H.; Ishikawa, K. Crystal structure of an acetylesterase from *Talaromyces cellulolyticus* and the importance of a disulfide bond near the active site. *FEBS Lett.* **2015**, *589*, 1200–1206. [CrossRef] [PubMed]

28. Correia, M.A.S.; Prates, J.A.M.; Brás, J.; Fontes, C.M.G.A.; Newman, J.A.; Lewis, R.J.; Gilbert, H.J.; Flint, J.E. Crystal structure of a cellulosomal family 3 carbohydrate esterase from *Clostridium thermocellum* provides insights into the mechanism of substrate recognition. *J. Mol. Biol.* **2008**, *379*, 64–72. [CrossRef] [PubMed]

29. Montanier, C.; Money, V.A.; Pires, V.M.R.; Flint, J.E.; Pinheiro, B.A.; Goyal, A.; Prates, J.A.M.; Izumi, A.; Stålbrand, H.; Morland, C.; et al. The active site of a carbohydrate esterase displays divergent catalytic and noncatalytic binding functions. *PLoS Biol.* **2009**, *7*, e1000071. [CrossRef] [PubMed]

30. Bae, S.Y.; Ryu, B.H.; Jang, E.; Kim, S.; Kim, T.D. Characterization and immobilization of a novel SGNH hydrolase (Est24) from *Sinorhizobium meliloti*. *Appl. Microbiol. Biotechnol.* **2013**, *97*, 1637–1647. [CrossRef] [PubMed]

31. Hwang, H.; Kim, S.; Yoon, S.; Ryu, Y.; Lee, S.Y.; Kim, T.D. Characterization of a novel oligomeric SGNH-arylesterase from *Sinorhizobium meliloti* 1021. *Int. J. Biol. Macromol.* **2010**, *46*, 145–152. [CrossRef] [PubMed]

32. Pei, J.; Kim, B.H.; Grishin, N.V. PROMALS3D: A tool for multiple protein sequence and structure alignments. *Nucleic Acids Res.* **2008**, *36*, 2295–2300. [CrossRef] [PubMed]

33. Gouet, P.; Robert, X.; Courcelle, E. ESPript/ENDscript: Extracting and rendering sequence and 3D information from atomic structures of proteins. *Nucleic Acids Res.* **2003**, *31*, 3320–3323. [CrossRef] [PubMed]

34. Otwinowski, Z.; Minor, W. Processing of X-ray diffraction data collected in oscillation mode. *Methods Enzymol.* **1997**, *276*, 307–326. [PubMed]

35. Ngo, T.D.; Ryu, B.H.; Ju, H.; Jang, E.J.; Kim, K.K.; Kim, T.D. Crystallographic analysis and biochemical applications of a novel penicillin-binding protein/β-lactamase homologue from a metagenomic library. *Acta Crystallogr. Sect. D Biol. Crystallogr.* **2014**, *70*, 2455–2466. [CrossRef] [PubMed]

36. Kantardjieff, A.K.; Rupp, B. Matthews coefficient probabilities: Improved estimates for unit cell contents of proteins, DNA, and protein-nucleic acid complex crystals. *Protein Sci.* **2003**, *12*, 1865–1871. [CrossRef] [PubMed]

37. Matthews, B.W. Solvent content of protein crystals. *J. Mol. Biol.* **1968**, *33*, 491–497. [CrossRef]

38. Weichenberger, X.C.; Rupp, B. Ten years of probabilistic estimates of biocrystal solvent content: New insights via nonparametric kernel density estimate. *Acta Crystallogr. Sect. D Biol. Crystallogr.* **2014**, *70*, 1579–1588. [CrossRef] [PubMed]

39. Adxv. *Adxv—A Program to Display X-ray Diffraction Images*; The Scripps Research Institute: La Jolla, CA, USA, 2013.

40. McCoy, A.J.; Grosse-Kunstleve, W.; Adams, P.D.; Winn, M.D.; Storoni, L.C.; Read, R.J. Phaser crystallographic software. *J. Appl. Crystallogr.* **2007**, *40*, 658–674. [CrossRef] [PubMed]

41. Afonine, P.V.; Grosse-Kunstleve, R.W.; Echols, N.; Headd, J.J.; Moriarty, N.W.; Mustyakimov, M.; Terwilliger, T.C.; Urzhumtsev, A.; Zwart, P.H.; Adams, P.D. Towards automated crystallographic structure refinement with phenix.refine. *Acta Crystallogr. D Biol. Crystallogr.* **2012**, *68*, 352–367. [CrossRef] [PubMed]

42. Emsley, P.; Cowtan, K. Coot: Model-building tools for molecular graphics. *Acta Crystallogr. D Biol. Crystallogr.* **2004**, *60*, 2126–2132. [CrossRef] [PubMed]